Improving atmospheric angular momentum forecasts by machine learning

R. Dill[1], J. Saynisch-Wagner[1], C. Irrgang[1], and M. Thomas[1,2]

[1]Earth System Modelling, Helmholtz Centre Potsdam, GFZ German Research Centre Potsdam, Germany.
[2]Institute of Meteorology, Freie Universität Berlin, Berlin, Germany.

Key Points:

- Motion terms of atmospheric angular momentum forecasts contain systematic errors
- Machine learning is used to learn and reduce these errors
- Remaining stochastic errors show modulations with a 24h period

Corresponding author: R. Dill, `dill@gfz-potsdam.de`

Abstract

Earth angular momentum forecasts are naturally accompanied by forecast errors that typically grow with increasing forecast length. In contrast to this behavior, we have detected large quasi-periodic deviations between atmospheric angular momentum wind term forecasts and their subsequently available analysis. The respective errors are not random and have some hard to define yet clearly visible characteristics which may help to separate them from the true forecast information. These kinds of problems, which should be automated but involve some adaptation and decision-making in the process, are most suitable for machine learning methods. Consequently, we propose and apply a neural network to the task of removing the detected artificial forecast errors. We found, that a cascading forward neural network model performed best in this problem. A total error reduction with respect to the unaltered forecasts amounts to about 30% integrated over a 6 day forecast period. Integrated over the initial 3 day forecast period, in which the largest artificial errors are present, the improvements amount to about 50%. After the application of the neural network, the remaining error distribution shows the expected growth with forecast length. However, a 24 hourly modulation and an initial baseline error of $2 * 10^{-8}$ became evident that were hidden before under the larger forecast error.

1 Introduction

The impact of atmospheric dynamics on the time-variable rotation of the Earth has been detected already during the early years of Very Long Baseline Interferometry (VLBI) by analyzing excitation functions based on global numerical weather prediction models (Barnes et al., 1983). Subsequently, the accuracy of space geodesy progressed rapidly, and also the quality of atmospheric model data sets improved due to newly available meteorological satellite observations and a break-through in meteorological data assimilation (Eubanks, 1993). Progress eventually led to the detection of signatures of the El Niño Southern Oscillation in seasonal variation in the length-of-day (Gross et al., 1996) caused by low-frequency variations in tropospheric winds.

Changes in the orientation of the solid Earth are conveniently studied by applying the principle of conservation of angular momentum in the whole Earth system including the surrounding fluid layers of atmosphere, oceans, and the terrestrial hydrosphere

(Gross, 2007). By summarizing the angular momentum changes from mass re-distributions in any of those sub-systems, the overall effect on the orientation of the solid Earth as represented by the terrestrial reference frame realized through a set of geodetic observatories is obtained. Changes in the mass distribution of the atmosphere can be expressed by its tensor of inertia calculated from given surface pressure fields. In addition, relative angular momentum changes can be derived from vertically integrated zonal and meridional atmospheric winds. The influence on Earth rotation from those angular momentum changes can be summarized as effective angular momentum functions (EAM) (Brzeziński, 1992) divided into the pressure or mass term and the motion term. EAM functions also consider a partly de-coupled rotation of the Earth's core, the effect of elastic Earth surface deformations under atmospheric pressure, and rotational deformations.

Numerous studies inter-compared EAM for the atmosphere with atmospheric angular momentum (AAM) from different sources (Koot et al., 2006; Masaki, 2008), and highlighted the importance of various specific aspects of the calculation of AAM including the accurate consideration of the surface orography (Zhou et al., 2006) and the consideration of stratospheric winds in addition to the tropospheric mass transports (Zhou et al., 2008). The individual contributions of surface pressure variations from regional sectors to AAM were also analyzed (Nastula et al., 2009), thereby opening up opportunities to principally inform atmospheric models by means of assimilating information on atmospheric angular momentum from geodetic observations (Neef & Matthes, 2012).

The strong relationship between model-based EAM and observed EOP encouraged the use of EAM forecasts for Earth rotation predictions. Especially, the short-term predictions of variations in the Earth spin rate UT1-UTC (universal time – coordinated universal time) could benefit from the 3rd component (χ_3) of AAM forecast data (Bell et al., 1991; Freedman et al., 1994). UT1 prediction errors were reduced by 20 % at a forecast horizon of 5 days. In 2000 the International Earth Rotation and Reference Systems Service (IERS) started to introduce AAM χ_3 forecasts from NCEP into their official Earth rotation prediction product Bulletin A in order to improve the short-term predictions of UT1-UTC variations. However, it showed up, that including the AAM forecasts sometimes degraded the UT1 prediction skill due to systematic differences between the AAM and UT1 series. Smoothing of the AAM data to reduce the sub-daily variability helped to reduce those effects (both periodic and linear).

Not only UT1 predictions could be improved by AAM χ_3 forecasts, but polar motion predictions could also benefit from AAM forecasts, namely the components χ_1 and χ_2. The first comparison campaign for Earth orientation parameters prediction underlines the necessity of the AAM forecast for the very-short-term EOP prediction (Kalarus et al., 2010). The authors also recommend the incorporation of EAM forecasts for ocean and terrestrial hydrology as presented the first time in a comprehensive study by Dill and Dobslaw (2010) for polar motion and UT1 predictions. The findings were confirmed by a study of Gross (2012) for improved UT1 predictions. Although EAM forecasts have typically a very short forecast horizon of only several days, 90-day EOP prediction could also benefit from the improvements in the very-first part of the EOP prediction (Dill et al., 2013, 2018).

EAM contributions for χ_1, χ_2, χ_3 mass and motion term forecasts of ocean and hydrology, χ_1 and χ_2 mass term forecasts of the atmosphere and χ_3 mass and motion forecast of the atmosphere show excellent prediction skills with a Brier-Skill (Storch & Zwiers, 1999) score above 0.8 throughout the whole forecast length of 6 days. In contrast to this good performance of most EAM components, AAM χ_1 and χ_2 motion term forecasts show much lower prediction skills. Here, regular drops below zero (Brier-Skill score $<$ 0.0) occur, see Fig. 3 in (Dobslaw & Dill, 2017). During the first 3 prediction days, these deficiencies in the AAM χ_1 and χ_2 motion term forecasts even drag down the overall EAM prediction skill sometimes below a Brier-Skill score of 0.8 that would be necessary for meaningful predictions.

In contrast to all other EAM forecast errors that are increasing with prediction length, large deviations between the AAM χ_1 and χ_2 motion term forecast and subsequently available analysis data pop up irregularly in the very-first forecast epochs. These deviations decrease with prediction length. Figures 1 and 2 exemplary show the deviations of 100 consecutive AAM motion term forecasts from its subsequently available analysis data. In the χ_1 and χ_2 components (Fig. 1) we find artificial quasi-periodic signals with initial amplitudes larger than the increasing stochastic forecast error after 6 days with an average period of 1.071 days in χ_1 and 1.098 days in χ_2. This artificial signal is excited irregularly from day to day with seemingly arbitrary amplitude and phase. The signal, if excited, vanishes with increasing forecast length. The χ_3 component (Fig. 2) reflects the normal behavior, a continuously increasing forecast error with increasing forecast length (compare temporal behavior along the vertical axis t_{forecast} in Fig. 1 and Fig. 2).

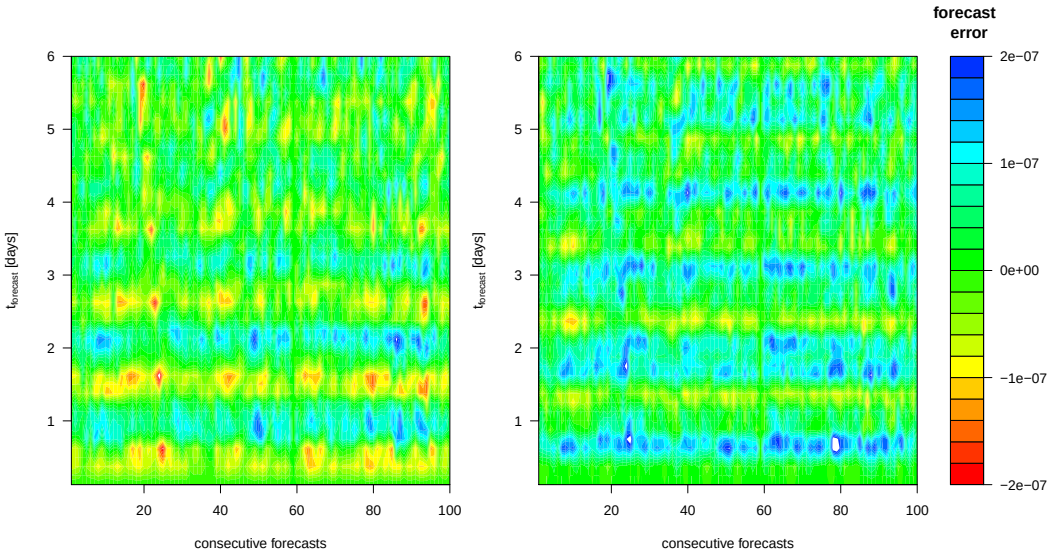

Figure 1. Systematic forecast errors in the χ_1 (right) and χ_2 (left) AAM motion terms. Forecast minus analysis time series. Heat map over 100 consecutive forecasts with a typical forecast time window of 6 days each (3-hourly sampling).

We suspect the origin of these AAM motion term forecast errors in the ECMWF (European Centre for Medium-Range Weather Forecasting) wind fields. So far, we couldn't find any documentation that might explain the existence of such artificial signals. It looks like the ECMWF's forecast system excites a free eigenmode once the system is no more constrained by assimilation data. In order to reduce the AAM forecast error, the following study explores machine learning (ML) to eliminate these supposedly artificial signals in the AAM motion term forecasts as far as possible. ML encompasses a class of generic yet highly adaptable operators and tools that can be trained to solve specific tasks. ML applications range from image classification, speech recognition to automated driving (e.g., Girasa, 2020). However, ML methods are also rapidly advancing in Earth sciences and can solve a plethora of classification, data-augmentation, inversion and modelling problems in this field (Irrgang et al., 2021; Salcedo-Sanz et al., 2020; Lary et al., 2016).

2 Atmospheric angular momentum analysis and forecast data

Atmospheric surface pressure and wind data are available from various sources including global re-analyses from the National Center for Environmental Prediction (NCEP),

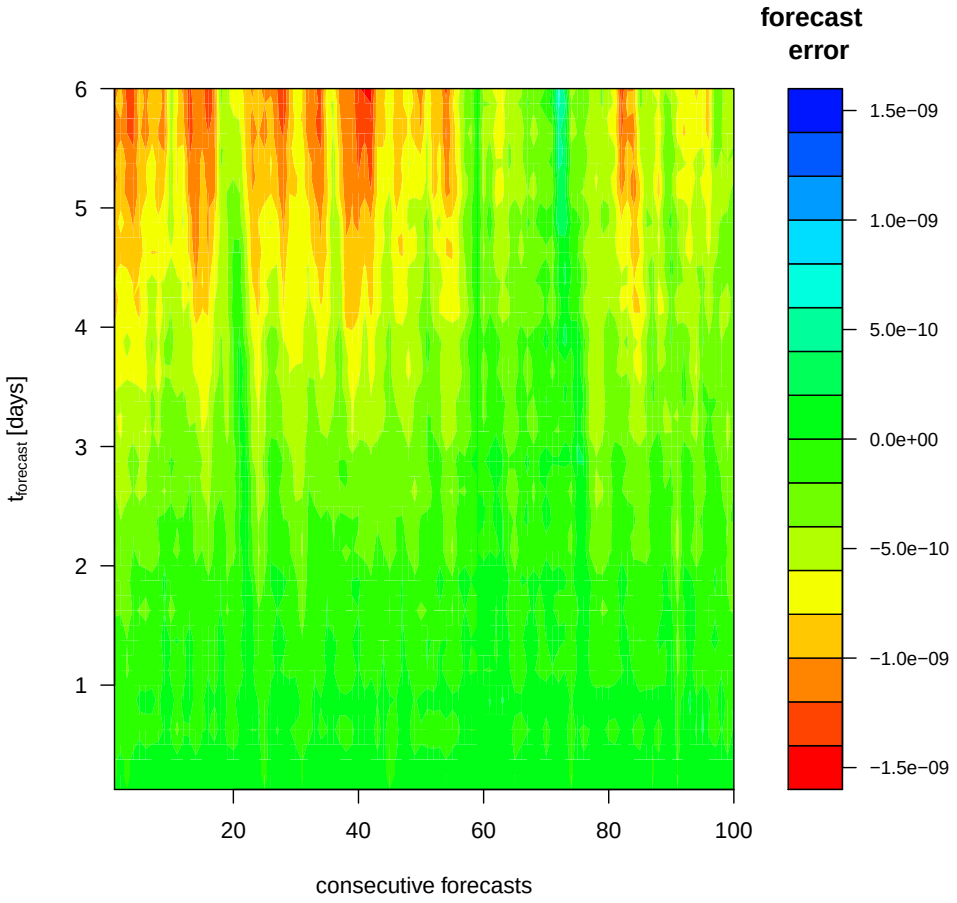

Figure 2. Systematic forecast errors in the χ_3 AAM motion term. Forecast minus analysis time series. Heat map over 100 consecutive forecasts with a typical forecast time window of 6 days each (3-hourly sampling).

the Japan Meteorological Agency, and the European weather agency ECMWF. Moreover, these institutions also provide short-term forecasts of atmospheric data, but generally the access to the data is restricted. AAM derived from NCEP data is processed at the center for Atmospheric and Environmental Research in Boston, and from ECMWF by ESMGFZ (Earth System Modelling group at the Helmholtz Centre Potsdam GFZ, German Research Centre for Geosciences). The AAM data products are provided via the International Earth Rotation and Reference Systems Service (IERS) under the auspices of the International Association of Geodesy (IAG). The IERS hosts the Global Geophysical Fluids Center (GGFC) that collects and disseminates those AAM data and metadata describing the contributions from mass re-distributions in atmosphere, oceans, and the terrestrial hydrosphere (https://www.iers.org/IERS/EN/DataProducts/GeophysicalFluidsData/geoFluids.htm
All data of the GGFC are publicly available without any charges.

In contrast to AAM (analysis) data sets from several re-analysis runs of numerical weather models, up to now, AAM forecasts data sets are publicly available via the GGFC only from ESMGFZ. Since 2016, ESMGFZ is moreover routinely providing EAM forecasts for either 6 days (individually for the EAM from atmosphee, ocean, hydrology and sea level) or 90 days (combination of all effects). The data sets are updated daily around 11:00 UTC with all time steps of the previous day (analysis) and 6 days into the future (forecasts). More details are available at http://esmdata.gfz-potsdam.de:8080/.

For this study, we collected 1988 daily AAM χ_1 and χ_2 motion term forecasts from 2016 - 2021, each sampled 3-hourly, i.e., 48 epochs for 6 days. The forecasts were contrasted against subsets of the AAM analysis data for the same epochs. Fig. 3 shows the mean differences time series and the variety of forecast errors over the forecast length. In contrast to Fig. 1 where individual forecast errors are plotted for a subset of consecutive forecasts, Fig. 3 shows the forecast errors for the whole data set in an aggregated view. Again, the strong quasi-periodicity of the χ_1 and χ_2 forecast errors is very prominent (Fig. 3, black line). However, the large variety of this quasi-periodicity in shape as well as period, phase, length and amplitude is visible, too (Fig. 3, grey swath).

On the one hand, exactly this erratic behavior makes it challenging to filter out this kind of error. Defining a filter that removes the error signal is challenging especially since the forecasts contain useful information on the same periods that has to be retained. As clearly as the errors are visible in the aggregated view of Fig. 3, when looking at a single forecast time series these periodic errors are far from obvious.

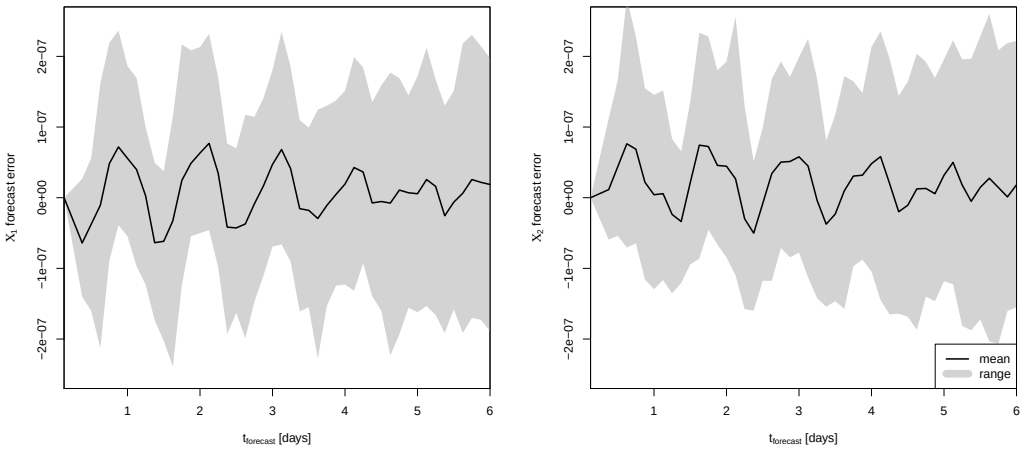

166 **Figure 3.** Forecast error, i.e., differences between AAM motion term forecast and the respec-
167 tive analyses time series for a prediction of 6 days into the future. Left: χ_1. Right: χ_2. Range
168 (grey) and average (black) over the 1988 individual curves.

162 On the other hand, the errors are not random and have some hard to define yet
163 clearly visible characteristics which may help to separate true from false forecast infor-
164 mation. With ML, a suitable filter has not to be defined a priori, it will be generated
165 within a neural network (NN) during the training.

169 In general, we would expect a forecast error increasing with forecast length. How-
170 ever, we can detect exceptionally large errors especially in the first forecast epochs (e.g.,
171 Fig. 3). The forecast errors are caused by an artificial periodic signal that is arbitrar-
172 ily excited at the beginning of the AAM forecasts with decreasing amplitude for longer
173 prediction length. Respective time series from AAM analysis do not contain this peri-
174 odic signal. In contrast to the AAM forecast, the AAM analysis is based on numerical
175 weather model simulations that assimilate observational data as soon as they are avail-
176 able.

177 In addition to the exceptional difference between AAM χ_1 and χ_2 motion term fore-
178 casts and analysis, we find also large deviations in the overlapping epochs of consecu-
179 tive forecasts. Here, we would expect only small deviations, especially for the first part
180 of the forecast period (e.g. 1st day of today's forecast vs. 2nd day of yesterday's fore-
181 cast). A preliminary approach to estimating the erroneous forecast signal from such con-

secutive forecasts and the known deviation from the analysis of older forecasts led only to a minor reduction of the overall forecast error as the overlapping time series are too short for a robust harmonic analysis.

Due to the restricted access to AAM forecasts from other numerical weather models such as NCEP, we could not inspect if the observed AAM motion term forecast shortcomings are typical for numerical weather prediction models or solely existent in ECMWF's atmospheric wind forecasts.

3 Methods

To isolate and remove the systematic errors contained in the polar motion related AAM data, different neural network classes were applied and tested: feed forward neural networks (FFNN), long short-term memory (LSTM) and other recurrent neural networks (RNN), as well as convolutional neural networks (CNN). As typical with ML approaches, the work includes a large fraction of trial and error to find suitable network architectures and connected hyper parameters like network shape, number of neurons in each layer, etc. We found that all of the listed network classes could be adapted to the problem and give comparable results (not shown). In the following, we describe only one of the tested ML classes, the cascading forward neural network model (CFN, e.g., Bolanča et al., 2009; Warsito et al., 2018). The CFN performed slightly better than the other tested configurations and was used to generate the results of this study. CFN are enhanced FFNN. In FFNN, while the first layer acts on the task-related input data, the following hidden layers process only the output of the previous layer. In a CFN, each hidden layer can access and process the output of all previous layers including the task-related input data.

The best performing CFN (MATLAB, 2021a) for our purpose is sketched in Fig. 4 and has the following layout, which was implemented using the Deep Learning Toolbox of MATLAB (MATLAB, 2021b). The CFN has 128 input neurons, which process AAM motion term forecasts for χ_1 and χ_2. Both input time series have a length of 64 epochs, each containing the erroneous 6-day forecast (48 epochs at 3-hourly sampling) and two days of preceding AAM analysis data (16 epochs). The network contains two hidden layers with 5 and 3 neurons, respectively, and a final output layer with 96 neurons, matching the length of the target forecast corrections for χ_1 and χ_2. The task of the CFN is

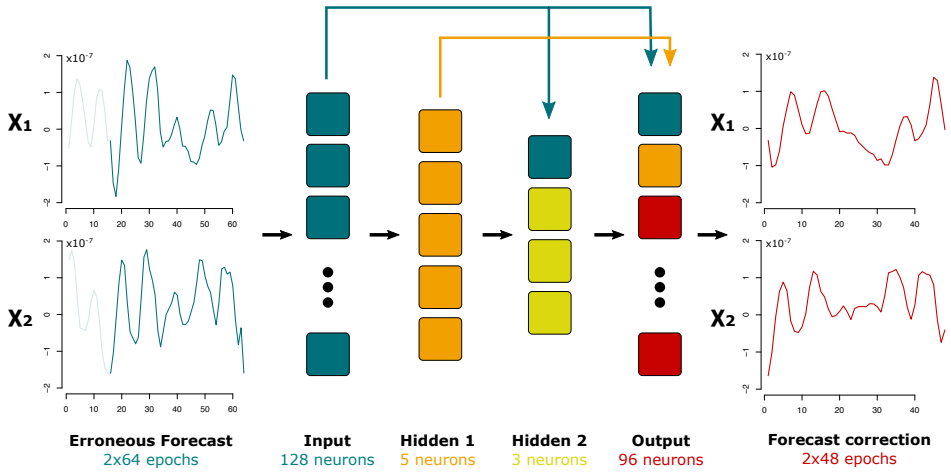

Figure 4. Sketch of the ML-based correction scheme for one exemplary AAM motion term forecast. The neural network analyzes time series of 6-day 3-hourly AAM motion term forecasts for χ_1 and χ_2 (dark blue time series), both complemented with 2 days from the latest analysis (light blue time series), to estimate an additive forecast correction (red time series). Colored blocks show neurons in the different layers and arrows indicate information aggregation and pathways between the layers.

to generate an additive forecast correction to derive an improved version of the erroneous input forecast. For this purpose, 6 days of differences (48 epochs), i.e., AAM forecast minus analysis for χ_1 or χ_2, are used as prescribed target outputs. To evaluate the ML-based correction, we compare erroneous and ML-corrected AAM forecasts with the corresponding AAM analysis time series in terms of root mean square errors (RMSE). During the training, the weights of the CFN are adapted by using the Levenberg-Marquardt back-propagation algorithm (Marquardt, 1963). From the available 1988 AAM forecasts (see sec. 2), 1500 forecasts and their subsequent analyses are used pair-wise during the CFN training and validation (Fig. 4). The remaining 488 forecasts and analyses are used to quantify the CFN performance with respect to data independent from the training procedure (see Sec. 4).

4 Results and Discussion

Figure 5 shows the results of the various CFN we designed to improve the AAM motion term forecasts. The results are shown as RMSE over the 488 time series which were refrained from the CFN training. The black lines corresponds to the black lines of

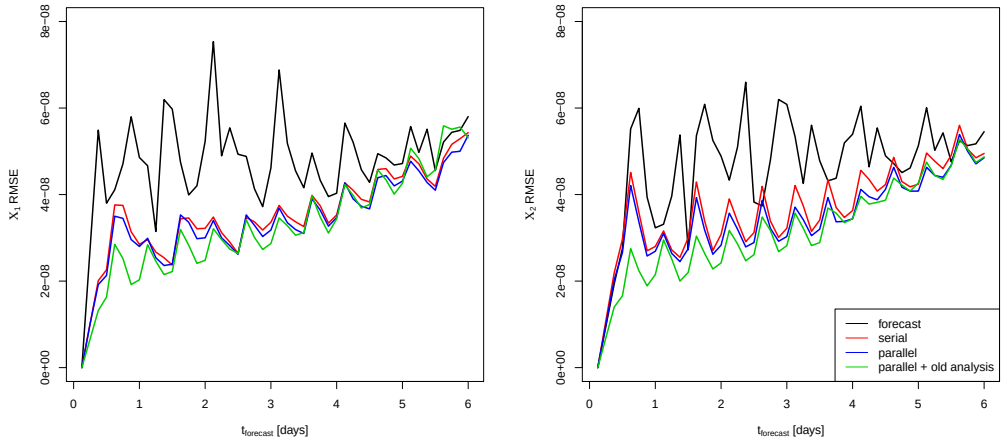

Figure 5. Performance comparison of traditional and CFN corrected AAM motion term forecasts. RMSE between forecast and analysis over the 488 time series which were refrained from the CFN training. Left: χ_1. Right: χ_2. Traditional uncorrected forecast (black), a serial CFN that separately processes χ_1 and χ_2 (red), a parallel CFN that simultaneously processes χ_1 and χ_2 (blue) and a parallel CFN that has analysis information (preceding the time of forecast) as additional input (green, cf. Fig. 4).

Fig. 3, i.e., this is the forecast error of the untreated AAM forecasts. Note that while Fig. 3 shows this baseline-error as temporal average, Fig. 5 represents a squared RMSE view.

The most basic approach to the problem is to train two CFN separately, one for χ_1 and one for χ_2. We call this the serial approach from now on. Here, each CFN takes one component of the AAM forecast as input and delivers a correction to it as output. In and output each have the same length of 48 epochs for 6 days. This most simple approach reduces already the RMSE significantly below the baseline (cf., Fig. 5, red with black line). The RMSE reduction is quite dramatic. The total RMSE of the 488 χ_1 (χ_2) forecasts amounts to $4,78 * 10^{-8}$ ($4,66 * 10^{-8}$) and is reduced by the serial approach to $3,53*10^{-8}$ ($3,67*10^{-8}$), i.e., an relative reduction of about 26% (21%). Especially in the first epochs of the forecast, where the supposedly artificial errors are most pronounced, the RMSE drop. The RMSE of the first 3 days of the forecast period (epochs 1-24) drop by 38% (30%). Consequently, by applying the serial approach, the remaining RMSE now grow more linear with the forecast horizon. Towards the end of the 6 days

forecasts, the RMSE of the serial approach and the RMSE of the unaltered forecasts meet. This linear RMSE trend is expected and far more realistic (cf. also Fig. 2) and arises naturally from chaotic and nonlinear components in the atmosphere system. In addition to the trend, an RMSE baseline of about $2*10^{-8}$ remains. The origin of this offset is not part of this study but may originate in missing or in-accurate assimilation data insufficiently constraining the ECMWF atmospheric model. Also remaining is a periodic modulation of the natural RMSE trend. The period of this remaining RMSE modulation is about 12 hours (corresponding to 24 hours in the non-squared errors) and might be connected with periodic daytime-dependent fluctuations in the quality of ECMWF's atmospheric forecasts compared to their operational analysis data. Given its input data, phase and amplitude of this remaining modulation is from the CFN point of view random and cannot be further reduced.

The next natural progression of the CFN was to process χ_1 and χ_2 together within one NN. This we termed parallel approach and this CFN has χ_1 and χ_2 as input and delivers respective corrections for both AAM motion term components (Fig. 5, blue line). Compared to the serial approach, the total RMSE do improve slightly: $3,42*10^{-8}$ ($3,46*10^{-8}$) for χ_1 (χ_2). That corresponds to an additional relative improvement of 3% (5%) compared with the serial approach. This is surprisingly little, given the fact that the information the CFN now gets is doubled. Naturally one would assume that since χ_1 and χ_2 are physically linked, information contained in the one could be useful for correcting the other. However, the influence of this additional information seems to be of minor importance as far as the filtering of the dominant AAM forecast errors is concerned. In other words, each component on its own contains already enough information to reduce the RMSE to certain degree and considering the other component gives only little additional, i.e., independent information.

However, additional information can indeed help to lower the RMSE further, e.g., by extending the input vectors of the parallel approach with analysis data that is available at the respective time of forecast. Here we add 16 epochs of data preceding the forecast time window as additional input to the CFN of the parallel approach (green, cf. Fig. 4). The results of this parallel-extended approach amount to a total RMSE of $3,29*10^{-8}$ ($3,19*10^{-8}$), i.e, a relative improvement with respect to the unaltered forecasts of 31% (32%) for the full 48 forecast epochs and 48% (45%) improvement when only the epochs 1-24 are considered (Fig. 5, green line).

Considering the remaining RMSE and their development with forecast time, the stochastic trend, the initial bias and the periodic modulation of the trend are now very clear in both polar motion AAM components. It seems that our general CFN approach has reached its full potential, given the provided information. In other words, from the perspective of the NN all remaining errors appear to be undecidable at forecast time. Undecidable in that sense that the error's governing mechanisms are random and completely external, i.e., no further robust hints about the errors can be found in the input data provided to the NN.

As a final note, the described results do not depend strongly on the choice of NN, the hyper-parameters, and the amount of training. As mentioned in Sec. 3, several NN classes were tested. All tried configurations were able to considerably reduce the RMSE of the forecasts. Likewise, all finally remaining RMSE showed the same characteristics as far as trend, modulation and bias are concerned. The RMSE values however, can differ slightly depending on the NN of choice and, as usual with ML, among several instances of the same network.

The purpose of an improved AAM motion term forecast is to enhance EOP predictions based on AAM forecasts. Without changing the EOP prediction system, three hindcast experiments with 1784 daily 90-day EOP predictions for the years 2016 - 2020 were calculated using ESMGFZ's EOP prediction algorithm (Dobslaw & Dill, 2017). The reference experiment was calculated with the original AAM forecasts. The second experiment uses the NN corrected AAM motion term forecasts. The third experiment uses 6-day subsets of the AAM analysis data to simulate perfect forecasts providing a target reference for the best possible EOP prediction that might be achieved without any further change (parameters for harmonic analysis and autoregression model) of the EOP prediction system. Table 1 summarizes the RMS prediction error for the three experiments for forecast horizons of 5, 10, 40, and 90 days. The polar motion x-component shows the expected improvement (4-5%), whereas the y-component shows almost no improvement. However, the y-component does also not benefit from a perfect forecast, which might be originated in the EOP prediction system that is tuned to the original forecasts and its included errors.

Table 1. Polar motion forecast error (RMS) in mas using original AAM forecasts (no correction), corrected AAM motion terms using NN (AAM corrected), and perfect forecasts reflecting the AAM analysis data. Forecast horizon 5, 10, 40, and 90 days into the future.

Polar motion forecast RMS [mas]		5 days	10 days	40 days	90 days
no correction	X pole	0.93	1.92	8.65	15.76
	Y pole	0.64	1.30	5.14	10.85
	pole	1.13	2.32	10.06	19.14
AAM corrected	X pole	0.89	1.83	8.64	15.78
	Y pole	0.67	1.33	5.09	10.77
	pole	1.12	2.26	10.03	19.11
perfect forecast	X pole	0.88	1.68	8.56	15.80
	Y pole	0.66	1.28	5.10	10.74
	pole	1.10	2.11	9.97	19.10

For a more extensive exploitation of the corrected AAM motion term forecasts, the harmonic analysis and autoregression model of the ESMGFZ's EOP prediction system has to be adapted to the new characteristics of the AAM motion terms.

5 Summary

The Earth System Modelling group at the Helmholtz Centre Potsdam GFZ, German Reserach Centre for Geosciences, (ESMGFZ) routinely provides effective angular momentum function (EAM) forecasts for the next 6 days, which are based on atmospheric reanalysis data from the European Centre for Medium-Range Weather Forecasts (ECMWF). EAM forecasts are naturally accompanied with forecast errors that typically grow with increasing forecast length. In contrast to this behavior, however, we have detected large quasi-periodic deviations between atmospheric angular momentum (AAM) χ_1 and χ_2 motion term forecasts and their subsequently available analysis. These supposedly artificial forecast errors appear to be excited irregularly with arbitrary amplitude and phase during the first forecast epochs and fade with increasing prediction length. While we could not conclusively isolate the cause of these artificial forecast errors, we suspect them to originate from artificial signatures in ECMWF's wind fields. Nevertheless, we expected

a significant improvement of the forecast quality during the first 3 to 4 days after separation and removal of the artificial errors.

The separation and removal of unwanted noise, or artificial errors, in otherwise meaningful data is a classical task for machine learning (ML). In this paper, we introduced a ML correction scheme for the AAM χ_1 and χ_2 motion term forecasts that dynamically derives a 6-day forecast correction for given 6-day AAM forecasts. After testing different neural network classes, a cascading forward neural network was chosen to isolate forecast errors from a six-year long time period (2016 - 2021) in a supervised training environment.

Comparing both ML-corrected and uncorrected AAM χ_1 (χ_2) forecasts with the subsequently available analysis has revealed a relative improvement of 31% (32%) for the entire 6-day forecast. During the first three forecast days, where the largest artificial errors were detected, a relative improvement of 48% (45%) could be achieved. Thus, we conclude that the neural network is able to successfully identify and remove the erroneous quasi-periodic forecast errors. Comparing the ML-corrected forecasts with their analysis, shows, as we would expect, a remaining forecast error trend that is increasing linearly with forecast length. On top, however, the error trend contains a remaining offset and an additional periodic modulation with an exact 24 hour (respectively 12 hours in the RMSE) period. These remaining signatures could not be entirely removed by the ML correction.

A more rigorous solution to get rid off systematic errors in the AAM motion term forecast could be the application of a likewise ML correction scheme in the underlying atmospheric wind field forecast rather than in the derived AAM terms.

However, even in its present form, the ML correction is already skillful enough to be included into the operational forecast system at GFZ, allowing us to provide significantly improved AAM forecasts to the community. In return, we hope that further analysis of our ML-based corrections and the described residual forecast errors can also feedback towards understanding and eliminating the causes of these artificial errors in the used atmospheric reanalysis products.

Acknowledgments

This study was in part funded by the Initiative and Networking Fund of the Helmholtz Association through the project "Advanced Earth System Modelling Capacity (ESM)". European Centre for Medium-Range Weather Forecasts, ECMWF, is acknowledged for providing atmospheric data from their operational models. Numerical simulations were performed at Deutsches Klimarechenzentrum, DKRZ, in Hamburg, Germany. The data sets analyzed in this study are publicly available from the Earth System Modelling group at GFZ (ESMGFZ angular momentum functions https://esmdata.gfz-potsdam.de:8080/repository).

The authors declare that they have no conflict of interests.

References

Barnes, R. T. H., Hide, R., White, A. A., & Wilson, C. A. (1983). Atmospheric angular momentum fluctuations, length-of-day changes and polar motion. *Proc. R. Soc. Lond., A Math. phys. sci.*, *387*(1792), 31–73. doi: 10.1098/rspa.1983.0050

Bell, M. J., Hide, R., & Sakellarides, G. (1991). Atmospheric angular momentum forecasts as novel tests of global numerical weather prediction models. *Philos. Trans. A Math. Phys. Eng. Sci.*, *334*, 55–92. doi: 10.1098/rsta.1991.0003

Bolanča, T., Stefanović, Š., Ukić, Š., & Rogošić, M. (2009). Development of temperature dependent retention models in ion chromatography by the cascade forward and back propagation artificial neural networks. *J. Liq. Chromatogr. Relat. Technol.*, *32*, 2765 - 2778.

Brzeziński, A. (1992, feb). Polar motion excitation by variations of the effective angular momentum function: considerations concerning deconvolution problem. *Manuscr. Geod.*, *17*, 3–20.

Dill, R., & Dobslaw, H. (2010, jun). Short-term polar motion forecasts from earth system modeling data. *J. Geodesy*, *84*(9), 529–536. doi: 10.1007/s00190-010-0391-5

Dill, R., Dobslaw, H., & Thomas, M. (2013, mar). Combination of modeled short-term angular momentum function forecasts from atmosphere, ocean, and hydrology with 90-day EOP predictions. *J. Geodesy*, *87*(198), 567–577. doi: 10.1007/s00190-013-0631-6

Dill, R., Dobslaw, H., & Thomas, M. (2018). Improved 90-day Earth orientation

predictions from angular momentum of atmosphere, ocean, and terrestrial hydrosphere. *J. Geodesy*, *92*. doi: 10.1007/s00190-018-1158-7

Dobslaw, H., & Dill, R. (2017). Predicting Earth Orientation Changes from Global Forecasts of Atmosphere-Hydrosphere Dynamics. *Adv. Space Res.*. doi: 10.1016/j.asr.2017.11.044

Eubanks, T. M. (1993). Variations in the orientation of the earth. In *Contributions of space geodesy to geodynamics: Earth dynamics* (p. 1-54). American Geophysical Union (AGU). doi: https://doi.org/10.1029/GD024p0001

Freedman, A. P., Steppe, J. A., Dickey, J. O., Eubanks, T. M., & Sung, L. Y. (1994). The Short-Term Prediction of Universal Time and Length-Of-Day Using Atmospheric Angular Momemtum. *J. Geophys. Res.: Solid Earth*, *99*(B4), 6981–6996. doi: 10.1029/93JB02976

Girasa, R. (2020). *Artificial Intelligence as a Disruptive Technology.* Palgrave Macmillan, Cham. doi: {https://doi.org/10.1007/978-3-030-35975-1}

Gross, R. S. (2012). Improving UT1 predictions using short-term forecasts of atmospheric, oceanic, and hydrologic angular momentum. *Proceedings Les Journees 2011*, 117–120. Retrieved from `https://syrte.obspm.fr/jsr/journees2011/pdf/gross.pdf`

Gross, R. S., Marcus, S. L., Eubanks, T. M., Dickey, J. O., & Kepenne, C. L. (1996). Detection of an ENSO signal in seasonal length-of-day variations. *Geophys. Res. Lett.*, *23*(23), 3373–3376. doi: 10.1029/96GL03260

Irrgang, C., Boers, N., Sonnewald, M., Barnes, E. A., Kadow, C., Staneva, J., & Saynisch-Wagner, J. (2021). Towards neural Earth system modelling by integrating artificial intelligence in Earth system science. *Nat. Mach. Intell.*, 667 - 674. doi: {10.1038/s42256-021-00374-3}

Kalarus, M., Schuh, H., Kosek, W., Akyilmaz, O., Bizouard, C., Gambis, D., ... Pasynok, C. S. (2010, sep). Achievements of the Earth orientation parameters prediction comparison campaign. *J. Geodesy*, *84*(10), 587–596. doi: 10.1007/s00190-010-0387-1

Koot, L., Viron, O. d., & Dehant, V. (2006). Atmospheric Angular Momentum Time-Series: Characterization of their Internal Noise and Creation of a Combined Series. *J. Geodesy*, *79*, 663–674. doi: 10.1007/s00190-005-0019-3

Lary, D. J., Alavi, A. H., Gandomi, A. H., & Walker, A. L. (2016). Machine

learning in geosciences and remote sensing. *Geosci. Front.*, *7*(1), 3-10. Retrieved from https://www.sciencedirect.com/science/article/pii/S1674987115000821 (Special Issue: Progress of Machine Learning in Geosciences) doi: https://doi.org/10.1016/j.gsf.2015.07.003

Marquardt, D. (1963). An Algorithm for Least-Squares Estimation of Nonlinear Parameters. *SIAM J. Appl. Math.*, *11*, 431–441.

Masaki, Y. (2008). Wind field differences between three meteorological reanalysis data sets detected by evaluating atmospheric excitation of earth rotation. *J. Geophys. Res.: Atmospheres*, *113*(D7). doi: https://doi.org/10.1029/2007JD008893

MATLAB. (2021a). *cascadeforwardnet.* Retrieved 2021-09-20, from {https://de.mathworks.com/help/deeplearning/ref/cascadeforwardnet.html}

MATLAB. (2021b). *Deep learning toolbox.* Natick, Massachusetts: The MathWorks Inc. Retrieved from https://de.mathworks.com/products/deep-learning.html

Nastula, J., Salstein, D., & Kolaczek, B. (2009). Patterns of atmospheric excitation functions of polar motion from highresolution regional sectors. *J. Geophys. Res.*, *114*(B4), B04407. doi: 10.1029/2008JB005605

Neef, L. J., & Matthes, K. (2012). Comparison of Earth rotation excitation in data-constrained and unconstrained atmosphere models. *J. Geophys. Res.*, *117*(D2), D02107. doi: 10.1029/2011jd016555

Salcedo-Sanz, S., Ghamisi, P., Piles, M., Werner, M., Cuadra, L., Moreno-Martanez, A., ... Camps-Valls, G. (2020). Machine learning information fusion in earth observation: A comprehensive review of methods, applications and data sources. *Inf. Fusion*, *63*, 256-272. doi: https://doi.org/10.1016/j.inffus.2020.07.004

Storch, H. v., & Zwiers, F. W. (1999). Forecast quality evaluation. In *Statistical analysis in climate research* (p. 391–406). Cambridge University Press. doi: 10.1017/CBO9780511612336.019

Warsito, B., Santoso, R., Yasin, S., & Yasin, B. (2018). Cascade Forward Neural Network for Time Series Prediction. *J. Physics: Conf. Series*, *1025*(012097). doi: 10.1088/1742-6596/1025/1/012097

Zhou, Y. H., Chen, J. L., & Salstein, D. A. (2008, 08). Tropospheric and strato-

spheric wind contributions to Earth's variable rotation from NCEP/NCAR reanalyses (2000–2005). *Geophys. J. Int.*, *174*(2), 453-463. doi: 10.1111/j.1365-246X.2008.03843.x

Zhou, Y. H., Salstein, D. A., & Chen, J. L. (2006). Revised atmospheric excitation function series related to earth's variable rotation under consideration of surface topography. *J. Geophys. Res.*, *111*. doi: 10.1029/2005J